arXiv:1601.06217v2 [cond-mat.mes-hall] 4 Aug 2016

Spatial dispersion of magnetic-edge magnetoplasmons: Effect of semi-infinite gate

O. G. Balev*
Departamento de Física, Universidade Federal do Amazonas, 69077-000, Manaus, Amazonas, Brazil

I. A. Larkin[2,3]
[2] *Department of Physics, Minho University, 4710-057, Braga, Portugal and*
[3] *Institute of Microelectronics Technology Russian Academy of Sciences, 142432 Chernogolovka, Russia*

(Dated: August 5, 2016)

Magnetic-edge magnetoplasmons (MEMPs) are obtained for a two-dimensional electron system (2DES) with atop semi-infinite metallic gate, at a distance d, and atop semi-infinite ferromagnetic film at a strong perpendicular magnetic field. For two most fast MEMPs, one with positive chirality and other with negative chirality, a strong spatial dispersion, due to effect of metallic half-plane gate, is obtained; some slower MEMPs manifest spatial dispersion too. Present MEMPs are localized at the magnetic-edge that is close to the wedge of metallic half-plane gate; the metallic wedge enhances localization of MEMPs at magnetic-edge. Obtained spatial dispersion has unconventional form. In particular, for two most fast MEMPs the phase velocities, ω/k_x, are the linear polynomials on the wave vector k_x in the long-wavelength region, $k_x d \ll 1$. Strong effect of the ferromagnetic film hysteresis on the MEMPs phase velocities and their anti-crossings are obtained for $0 < k_x d \leq 1$. Two MEMPs of opposite chirality, especially two most fast MEMPs, at some resonance frequency can create a resonance circuit, with closed wave path along a fraction of the magnetic edge perimeter, with a total change of the wave phase given by an integer of 2π.

PACS numbers: 73.21.-b, 75.75.-c, 73.20.Mf, 73.43.Lp

I. INTRODUCTION

Different types of "density gradient" edge magnetoplasmons (EMPs) have been studied for (conventional) 2DES [1–17] subjected to a strong homogeneous magnetic field; for a discussion of previous publications, e.g., see [1]. These EMPs appear due to a strong change of the stationary local electron density at the edge of the channel (in particular, in the vicinity of edge states) that induces a strong modulation of the local magnetoconductivity tensor; modulation of the nondiagonal components is especially important [1, 2, 5, 8, 9, 13]. In addition, EMPs in graphene have attracted attention recently [18–25].

As a rule, EMPs are studied at a long-wavelength region $k_x a_{EM} \ll 1$, [1, 4–10, 13] where a_{EM} is a finite characteristic scale; it is understood that another characteristic scale $1/k_x$, related with the wavelength $2\pi/k_x$, also is involved. Typically a_{EM} is the characteristic localisation, along y, for a charge density of the most fast EMP; for different models of EMPs the value of a_{EM} can be quite different as well as the physical picture involved [1, 5, 8–10, 13]. For a homogeneous sample without the gate, in the long-wavelength region, only the fundamental EMP (the only EMP in the model of Ref. [1]; notice, this EMP in Ref. [5] is called as *the conventional edge magnetoplasmon mode*) shows spatial dispersion as a weak logarithmic dependence of the phase velocity [1–3, 5, 8, 9, 13] on k_x, $\omega/k_x \propto \ln(1/k_x a_{EM})$. In addition, here the phase velocities of the rest of EMPs are independent of k_x and smaller [5, 8, 9, 13]. Often, these dispersionless modes are called as acoustic EMPs [5]. If a plane metallic gate is present at a distance d from the 2DES then all EMPs are dispersionless for $k_x d \ll 1$, as their phase velocities are independent of k_x [6, 8, 9, 13].

Recently,[26, 27] the chiral modes in the homogeneous 2DES (localized at $z = 0$ plane in GaAs based sample, with a very thing homogeneous nonmagnetic metallic gate above it, at $z = d$) induced by "magnetic gradient" have been obtained theoretically. Laterally inhomogeneous strong magnetic field within the plane of 2DES appears due to ferromagnetic semi-infinite film ($y \leq 0$) of a finite thickness, located atop of the gate. Named as magnetic-edge magnetoplasmons (MEMPs), these modes are localized, along the $y-$direction, on the characteristic scale d in a vicinity of $y = 0$; i.e., in the principal region of magnetic field inhomogeneity [26, 27]. For $k_x d \ll 1$ all these MEMPs show acoustic dispersion [26, 27]. I.e., for a plane metallic gate all MEMPs are dispersionless in the long-wavelength region. Notice, any MEMPs are absent if a strong magnetic field applied to 2DES is spatially homogeneous [26, 27].

In present study we consider the effect on MEMPs by a half-plane metallic gate (HPMG), at ($y < 0$, $z = d$). Schematic view of the model geometry, otherwise similar to the one of Refs. [26, 27], is shown in Fig. 1. Here 2DES, at $z = 0$, is embedded in GaAs based sample, with the dielectric constant ε, that occupies a half-space $z < d$. As the semi-infinite gate, i.e., HPMG, is assumed very thin it is not shown explicitly in Fig. 1. 2DES is subjected to a strong laterally inhomogeneous magnetic field $\mathbf{B}(y) = B(y)\hat{\mathbf{z}}$, which appears due to ferromagnetic

*Electronic address:ogbalev@ufam.edu.br

semi-infinite film of a finite thickness ηd. A strong external spatially homogeneous magnetic field $\mathbf{B}_{ext} = B_{ext}\hat{\mathbf{z}}$ is applied as well.

Qualitative and strong quantitative effects of HPMG on some MEMPs are obtained. In particular, a strong spatial dispersion of unconventional form, for two MEMPs of opposite chirality, is obtained for $k_x d \ll 1$.

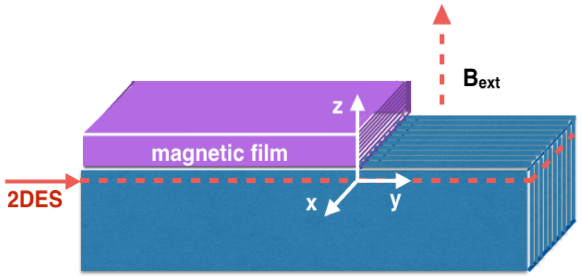

Figure 1: (Color online) Sketch of model geometry: 2DES, at $z = 0$, is embedded in a dielectric medium. The ferromagnetic semi-infinite film is located at $y < 0$, $d < z < d(1+\eta)$; HPMG, at $y < 0$, $z = d$, is not shown.

In Sec. II we present further attributes of the model for MEMPs in 2DES with half-plane atop metallic gate and then the advanced attributes of the model and pertinent basic relations. Then in Sec. III we present results for spatial dispersion of MEMPs, effect of hysteresis, anticrossings. In Sec. IV we make concluding remarks.

II. MAGNETIC-EDGE MAGNETOPLASMONS FOR HALF-PLANE GATE: FORMALISM

A. Model attributes: Introduction

It is assumed that for any actual spatially homogeneous (in particular, zero) effective magnetic field B applied to 2DES, we have spatially homogeneous 2DES of a constant area density n_I as well as the ions jellium background with the same area density, n_I. Spatially inhomogeneous effective magnetic field $B(y)$ is assumed as a smooth function of y, with the characteristic scale Δy. Comparing the perturbation of the electron density due to spatially inhomogeneous magnetic field from its unperturbed value n_I, it follows that the density of 2DES is very weakly modified if the Bohr radius $a_B \ll 2\Delta y$ and the quantum magnetic length $\ell_0(y) \ll 2\Delta y$; $a_B = \hbar^2/m^* e^2$, $\ell_0(y) = \sqrt{\hbar c/|e|B(y)}$, where m^* is an effective mass of 2D electrons. Below we assume that these conditions are satisfied and, respectively, the static electron density is taken as n_I.

We assume, cf. with Fig. 1, a constant magnetic moment for the ferromagnetic semi-infinite film $\mathbf{M}_0 = M_0\hat{\mathbf{z}}$; $M_0 > 0$ if otherwise is not stated. Then readily it follows [26, 28] that

$$B(y) = B_{ext} - 2M_0\{\arctan(Y) - \arctan(Y/(1+\eta))\}, \quad (1)$$

where $Y = y/d$; i.e., in present study $\Delta y = d$. Point out that in Eq. (1) in the SI units M_0 is changed on $\mu_0 M_0/(4\pi)$. Notice, in experiments with GaAs-based 2DES the values of d and ηd can be ~ 100nm [29]. External spatially homogeneous magnetic field $B_{ext} > 0$, if otherwise is not stated, is applied as well.

We assume that the low-frequency, $\omega \ll \omega_c$, and the long-wavelength, $k_x \ell_0(y) \ll 1$, conditions are satisfied. Then the wave current density in the quasi-static approximation (e.g., cf. with Ref. [8, 9, 30]) is given as

$$j_x(y) = \sigma_{xx}(y)E_x(y) - \sigma^0_{yx}(y)E_y(y),$$
$$j_y(y) = \sigma_{yy}(y)E_y(y) + \sigma^0_{yx}(y)E_x(y), \quad (2)$$

where we have suppressed the exponential factor $\exp[-i(\omega t - k_x x)]$; arguments ω, k_x in $j_\mu(y)$, $E_\mu(y)$ are omitted, to simplify notations. We will neglect by a dissipation assuming a clean 2DES and sufficiently low temperatures T.

In the absence of metallic gates and for homogeneous background dielectric constant ε, using Eq. (1), the Poisson equation and the linearized continuity equation, we obtain for the wave charge density $\rho(\omega, k_x, y)$ the integral (cf. with Ref. [8, 9, 30]) equation

$$-i\omega\rho(\omega, k_x, y) - i\frac{2}{\varepsilon}\{k_x \frac{d}{dy}[\sigma^0_{yx}(y)]\}$$
$$\times \int_{-\infty}^{\infty} dy' K_0(|k_x||y - y'|)\rho(\omega, k_x, y') = 0, \quad (3)$$

where $G^{(0)}(k_x, y - y', z = 0; z' = 0) = (2/\varepsilon)K_0(|k_x||y - y'|)$ is the Fourier transform over the coordinate $\Xi = x - x'$ of the Green function at $(x, y, z = 0)$ for the unit charge localized at $(x', y', z' = 0)$; $K_0(x)$ is the modified Bessel function. In the model of Refs. [26, 27] is assumed that in addition to the semi-infinite magnetic film, a very thin infinite metallic nonmagnetic film of the thickness $\ll d$ is places on the top of the sample at a distance d from the 2DES. Then the kernel K_0 in Eq. (3) is replaced by

$$R^{(1)}_g(|y - y'|\ ,\ k_x; d) = K_0(|k_x||y - y'|)$$
$$-K_0(|k_x|\sqrt{(y - y')^2 + 4d^2}), \quad (4)$$

here the Green function $G^{(1)}(k_x, y - y', z = 0; z' = 0) = (2/\varepsilon)R^{(1)}_g(|y - y'|, k_x; d)$.

In present model HPMG is a half-plane metallic nonmagnetic film of negligible thickness. Besides HPMG and the plane of 2DES the rest of space presents dielectric background with spatially homogeneous dielectric constant ε. Henceforth the ferromagnetic semi-infinite film is taken as a dielectric too, with dielectric constant ε.

B. Basic Relations and Advanced Attributes of the Model

For the present model, with HPMG, we obtain the integral equation for MEMPs, cf. with Eq. (14) of Ref.

[27], as

$$W\rho(\omega,k_x,X)-g_0(X)f_0(X)\int_{-1}^{1}dX' \times\widetilde{G}^{(2)}(k_x;d\tan(\frac{\pi}{2}X),z=0;d\tan(\frac{\pi}{2}X'),z'=0) \times\frac{(\pi/2)}{\cos^2(\pi X'/2)}\rho(\omega,k_x,X')=0, \quad (5)$$

where $W=\omega/(k_xv_0)$ is the dimensionless phase velocity and its sign corresponds to the chirality of a wave, i.e., $W>0$ ($W<0$) for positive (negative) chirality if $v_0>0$. Here $v_0=|e|cn_I/(\varepsilon B_0)$ is a characteristic velocity of the problem with $B_0=B_{ext}^2/(4M_0)$. Further, $X=\frac{2}{\pi}\arctan(Y)$ [$X'=\frac{2}{\pi}\arctan(Y')$] is a new variable that change from -1 to 1 as Y [Y'] changes from $-\infty$ to ∞,

$$g_0(X)=\{\frac{1+\eta}{(1+\eta)^2+\tan^2(\pi X/2)}-\frac{1}{1+\tan^2(\pi X/2)}\} \quad (6)$$

is a dimensionless gradient of $B(y)$, and the factor

$$f_0(X)=\{1-\frac{2M_0}{B_{ext}}[\frac{\pi}{2}X-\arctan(\frac{1}{1+\eta}\tan(\frac{\pi}{2}X))]\}^{-2}. \quad (7)$$

Point out that $g_0(X)$ is the symmetric function of X as function $f_0(X)$ is neither symmetric nor antisymmetric. Here $\widetilde{G}^{(2)}(k_x;y,z=0;y',z'=0)\equiv(\varepsilon/2)G^{(2)}(k_x;y,z=0;y',z'=0)$, where $G^{(2)}(k_x;y,z=0;y',z'=0)$ is the Fourier transform, over the coordinate $\Xi=x-x'$, of the Green function at $z=0$ plane (of 2DES) for the unit charge localized at $(x',y',z'=0)$. In what follows we will use notations $\Delta_\varphi(k_x,X,X')\equiv\widetilde{G}^{(2)}(k_x;d\tan(\frac{\pi}{2}X),z=0;d\tan(\frac{\pi}{2}X'),z'=0)$, and

$$\Delta_\varphi(k_x,X,X')=\int_0^\infty d\xi\cos(k_xd\,\xi)\widetilde{\Delta}_\varphi(\xi,X,X'), \quad (8)$$

where dimensionless variable $\xi=\Xi/d$ is introduced. Using the analytical solution for the electric potential potential of the point charge nearby the wedge of conducting half-plane in a vacuum, e.g., see [31], we straightforwardly obtain that

$$\widetilde{\Delta}_\varphi(\xi,X,X')=\frac{1}{\pi}\Big\{[\xi^2+(\tan(\frac{\pi}{2}X')-\tan(\frac{\pi}{2}X))^2]^{-1/2} \times\arccos[-\frac{\cos(\pi(X'-X)/4)}{\cosh(\chi/2)}] -\Big[\xi^2+4+(\tan(\frac{\pi}{2}X')-\tan(\frac{\pi}{2}X))^2\Big]^{-1/2} \times\arccos[\frac{\sin(\pi(X'+X)/4)}{\cosh(\chi/2)}]\Big\}, \quad (9)$$

where

$$e^\chi=\left\{\left[\frac{\xi^2+2+\tan^2(\frac{\pi}{2}X')+\tan^2(\frac{\pi}{2}X)}{2\sqrt{1+\tan^2(\frac{\pi}{2}X')}\sqrt{1+\tan^2(\frac{\pi}{2}X)}}\right]^2-1\right\}^{1/2} +\frac{\xi^2+2+\tan^2(\frac{\pi}{2}X')+\tan^2(\frac{\pi}{2}X)}{2\sqrt{1+\tan^2(\frac{\pi}{2}X')}\sqrt{1+\tan^2(\frac{\pi}{2}X)}}. \quad (10)$$

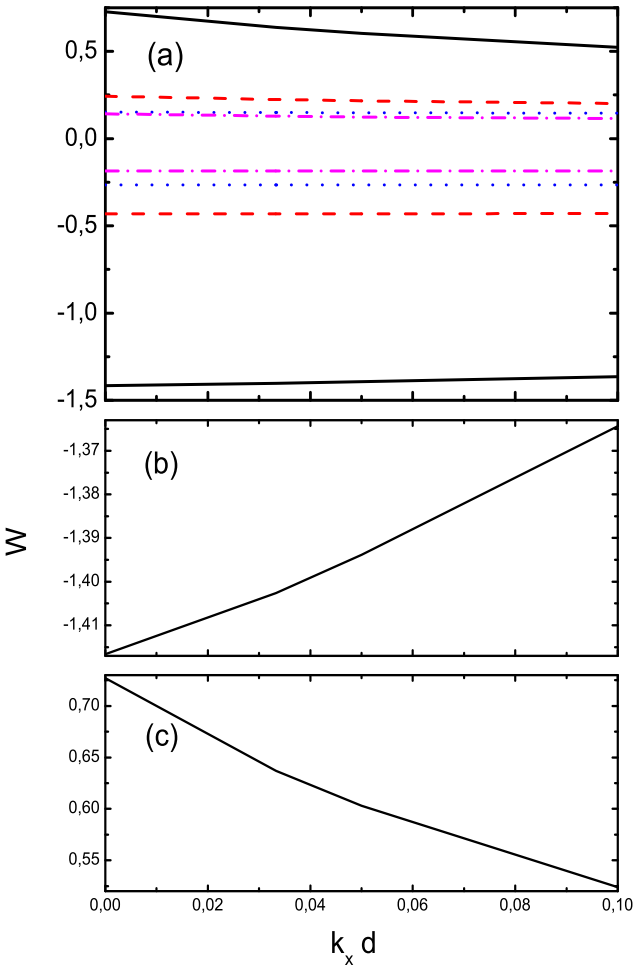

Figure 2: (Color online) Dimensionless phase velocity $W=\omega/k_xv_0$ as function of k_xd at a long-wavelength region $0.1\geq k_xd>0$ for $\eta=1$, $2M_0/B_{ext}=0.5$, $B_{ext}=0.6$T, $v_0>0$. Figs. 2(a), 2(b), and 2(c) show: (a) four fastest MEMPs among the modes with the positive (negative) chirality, (b) zoom for the fastest MEMP with the negative chirality, and (c) zoom for the fastest MEMP with the positive chirality.

For $k_x\to0$ we also obtain $\Delta_\varphi(k_x=0,X,X')$ in the form different from the integral form of Eq. (8). It is given as

$$\Delta_\varphi(k_x=0,X,X')=-\Re\{\ln \left[\frac{(\tan(\frac{\pi}{2}X)-i)^{1/2}-(\tan(\frac{\pi}{2}X')-i)^{1/2}}{(\tan(\frac{\pi}{2}X)-i)^{1/2}+(\tan(\frac{\pi}{2}X')+i)^{1/2}}\right]\Big\}= -\frac{1}{2}\ln\left\{\frac{(Z_+(X)-Z_+(X'))^2+(Z_-(X)-Z_-(X'))^2}{(Z_+(X)+Z_+(X'))^2+(Z_-(X)-Z_-(X'))^2}\right\}, \quad (11)$$

where $Z_\pm(t)=[2\sqrt{\tan^2(\pi t/2)+1}\pm2\tan(\pi t/2)]^{1/2}$. Point out, Eq. (11) is equivalent to Eq. (8) for $k_x=0$.

From Eqs. (5)-(9) it follows that a solution of the

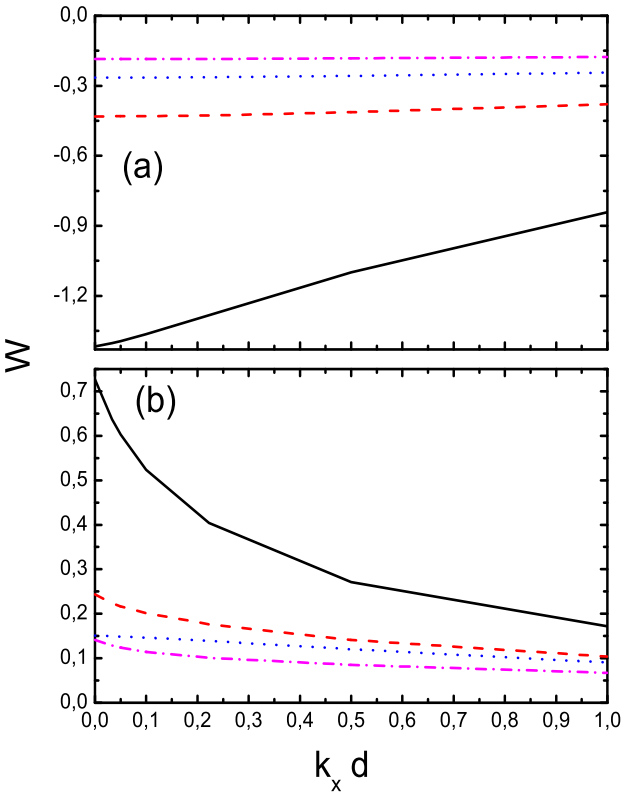

Figure 3: (Color online) Dimensionless phase velocity W as function of $k_x d$ at a wide region $1.0 \geq k_x d > 0$ for parameters of Fig. 2. Figs. 3(a) and 3(b) show four fastest MEMPs among the modes with the negative and the positive chirality, respectively.

integral equation Eq. (5) is not either symmetric or antisymmetric. We look for a solution of Eq. (5) in the form

$$\rho(\omega, k_x; X) = g_0(X) f_0(X) \{ \sum_{n=0}^{N_0} a_n(\omega, k_x) \left[\cos(n\pi X) - \frac{1}{2}\delta_{n,0} \right] + \sum_{n=N_0+1}^{2N_0+1} a_n(\omega, k_x) \sin\left[(n - N_0)\pi X\right] \}, \quad (12)$$

which for $N_0 \to \infty$ is exact as pertinent basis of the orthonormal functions becomes complete.

For a finite N_0, Eq. (12) is an expansion over the set of $(N_0 + 1)$ symmetric and $(N_0 + 1)$ antisymmetric orthonormal functions. Now Eq. (5) we reduce to the system of $2(N_0+1)$ linear homogeneous equations. The first $(N_0 + 1)$ equations, for $m = 0, 1, 2, ..., N_0$, are obtained by multiplying Eq. (5) on $\cos(m\pi X)/[g_0(X) f_0(X)]$ and then integrating over X, $\int_{-1}^{1} dX ...$, as follows

$$W a_m - \{ \sum_{n=0}^{N_0} r_{m,n} a_n + \sum_{n=N_0+1}^{2N_0+1} r_{m,n} a_n \} = 0, \quad (13)$$

The other $(N_0 + 1)$ equations, for $m = N_0 + 1, N_0 + 2, ..., 2N_0 + 1$, are obtained after multiplying Eq. (5) by $\sin\left[(m - N_0)\pi X\right] / (g_0(X) f_0(X))$ and then integrating over X. As a result we obtain the system of equations that formally can be obtained from Eq. (13) by pertinent change in the values of m. Finally, the system of $2(N_0 + 1)$ linear homogeneous equations is given as

$$W a_m - \sum_{n=0}^{2N_0+1} r_{m,n} a_n = 0, \quad (14)$$

where $m, n = 0, 1, 2, 3, ..., 2N_0 + 1$. The matrix elements $r_{mn} = I^{(1)}_{mn}$ for $(m \leq N_0,\ n \leq N_0)$, $r_{mn} = I^{(2)}_{mn}$ for $(m \geq N_0 + 1,\ n \leq N_0)$, $r_{mn} = I^{(3)}_{mn}$ for $(m \leq N_0,\ n \geq N_0 + 1)$, $r_{mn} = I^{(4)}_{mn}$ for $(m \geq N_0 + 1,\ n \geq N_0 + 1)$ are given by Eqs. (A1)-(A4) in Appendix A, where, in particular, an integral over X (X') from -1 to 1 is transformed to the interval from 0 to 1.

For a nontrivial solution Eq. (12) the determinant of the $2(N_0 + 1) \times 2(N_0 + 1)$ matrix of Eq. (14) must be equal to zero. This gives $2(N_0 + 1)$ dispersion relations for dimensionless phase velocities $W = W_j(k_x)$, $j = 1, 2, ..., 2(N_0 + 1)$ of the first $2(N_0 + 1)$ MEMPs branches. These dispersion relations readily can be rewritten in a more usual form $\omega = \omega_j(k_x)$. Then, e.g., for $N_0 = 1$ the first four MEMPs are obtained and for $N_0 = 2$ we will obtain the first six MEMPs, however, only two of them are new modes as other four solutions give previously obtained four MEMPs with better precision. With further increase in N_0 we will calculate, in particular, these first four MEMPs too, noteworthy, with fast growing precision.

III. SPATIAL DISPERSION OF MAGNETIC-EDGE MAGNETOPLASMONS. EFFECT OF A HYSTERESIS

A. Magnetic edge magnetoplasmons for $B_{ext} > 0$, $M_0 > 0$ and $B_{ext} < 0$, $M_0 < 0$

1. *Magnetic edge magnetoplasmons for $B_{ext} > 0$, $M_0 > 0$*

In Fig. 2(a) we present the dispersion relations for dimensionless phase velocities, $W = W_j(k_x)$, of four fastest MEMP modes $|W^{(n)}_1| > |W^{(n)}_2| > ... > |W^{(n)}_4|$ with the negative chirality, $W < 0$, and of four fastest MEMP modes with the positive chirality, $W^{(p)}_1 > W^{(p)}_2 > ... > W^{(p)}_4 > 0$. Fig. 2 is plotted for $\eta = 1.0$, and $2M_0/B_{ext} = 0.5$; the latter for $B_{ext} = 0.6$T implies that $M_0 = B^2_{ext}/(4B_0) = 3/20$T for $B_0 = 0.6$T. Fig. 2(b) presents a zoom of the dispersion relation $W^{(n)}_1(k_x) \approx 0.53\, k_x d - 1.417$ and it is seen that $W^{(n)}_1(k_x)$ very close follow the linear dependence, on k_x; according to Fig. 2(a), the rest three MEMPs of the negative chirality have negligible spatial dispersion in present long-wavelength region as their $W^{(n)}_j(k_x)$, $j = 2, 3, 4$, are practically independent of k_x. Fig. 2(c) presents a zoom of the disper-

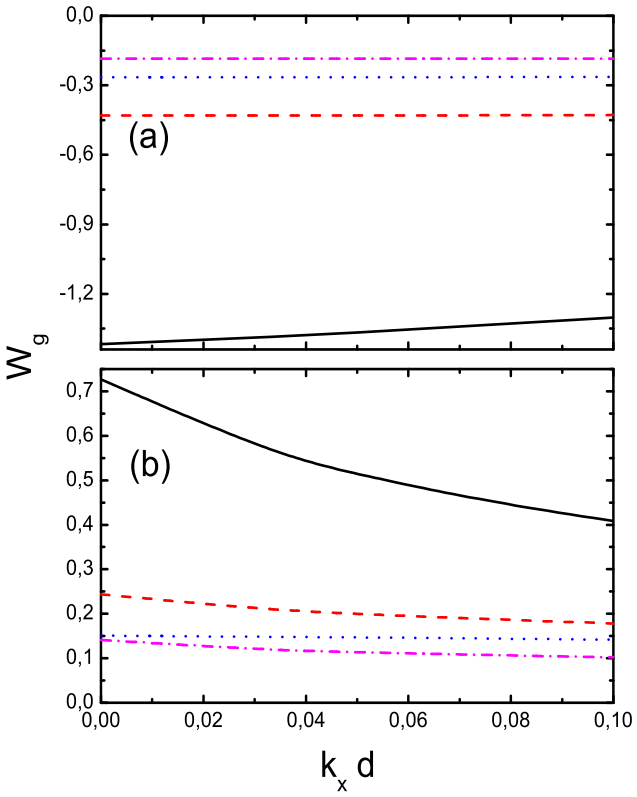

Figure 4: (Color online) Dimensionless group velocity W_g as function of $k_x d$ at a long-wavelength region $0.1 \geq k_x d > 0$ for the eight waves of Fig. 2; $\eta = 1$, $2M_0/B_{ext} = 0.5$, $B_{ext} = 0.6$T.

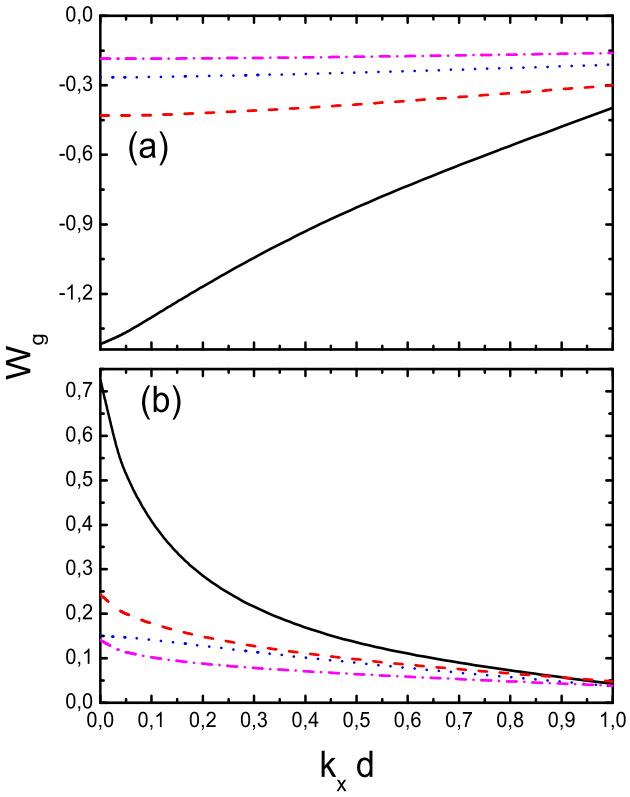

Figure 5: (Color online) Dimensionless group velocity W_g as function of $k_x d$ at $1.0 \geq k_x d > 0$ for parameters of Fig. 2. Fig. 5(a) and Fig. 5(b) show MEMPs with the negative and the positive chirality.

sion relation $W_1^{(p)}(k_x) \approx -2.03\, k_x d + 0.727$ which rather closely follow the linear dependence on k_x; in addition, it is much steeper than in Fig. 2(b). The rest of MEMPs with the positive chirality $W_j^{(p)}(k_x)$, $j = 2, 3, 4$, in Fig. 2(a) have an essential spatial dispersion of qualitatively the same form as $W_1^{(p)}(k_x)$, however, with much smaller dependence on k_x. Results for MEMPs presented in Fig. 2 (and other figures of the work) correspond to a very good convergence for used $N_0 = 11$; here from the 24×24 matrix system of equations we obtain 24 MEMPs.

Point out that here without the ferromagnetic film (with the same direction of $\mathbf{B}_{ext}$) for a usual type of the edge at $y = 0$, due to a monotonic decrease of the electron density for increasing y, it follows [5, 30] that $W < 0$ for all EMPs; i.e., the EMPs have the same negative chirality as present $W_i^{(n)}$ MEMPs.

In Fig. 3a and Fig. 3b we present the dispersion relations, $W = W_j(k_x)$, for eight MEMPs shown in Fig. 2a at a wider region $1.0 \geq k_x d > 0$. It is seen in Fig. 3b that $W_1^{(p)}(k_x)$ for $1 \geq k_x d \gg 0.1$ essentially changes its dependence on k_x from a linear one to approximately $\propto k_x^{-1}$, however, in Fig. 3a the changes for $W_1^{(n)}(k_x)$ are rather small. In addition, Fig 3a shows that only at $k_x d \sim 1$ velocities $W_j^{(n)}(k_x)$, $j = 2, 3, 4$, become a weakly dependent on k_x.

In Fig. 4(a) and Fig. 4(b) we present dimensionless group velocity, $W_g(k_x) = d\, \omega_j(k_x)/(v_0 dk_x)$, for MEMPs shown in Fig. 3(a) and Fig. 3(b), at the long-wavelength region $0.1 \geq k_x d > 0$. In addition, in Fig. 5(a) and Fig. 5(b) we present dimensionless group velocity, W_g, for MEMPs shown in Fig. 3(a) and Fig. 3(b), at a wide region $1.0 \geq k_x d > 0$.

In Fig. 6 for $\eta = 2$ we plot the same dependences as in Fig. 2 for parameters that coincide, except of η, with those of Fig. 2. In Fig. 6(a) we present the dispersion relations for the dimensionless phase velocities, $W = W_j(k_x)$, of four fastest MEMP modes $|W_1^{(n)}| > |W_2^{(n)}| > ... > |W_4^{(n)}|$ of the negative chirality and of four fastest MEMP modes of the positive chirality, $W_1^{(p)} > W_2^{(p)} > ... > W_4^{(p)} > 0$. Fig. 6(b) and Fig. 6(c) present a zoom of the dispersion relation $W_1^{(n)}(k_x) \approx 0.89\, k_x d - 2.183$ and $W_1^{(p)}(k_x) \approx -4.00\, k_x d + 1.271$, respectively.

In Fig. 7(a) and Fig. 7(b) we present the dispersion relations, $W = W_j(k_x)$, for eight MEMPs shown in Fig. 6(a) at a wider region $1.0 \geq k_x d > 0$. It is seen in Fig. 7(b) that $W_1^{(p)}(k_x)$ for $1 \geq k_x d \gg 0.1$ essentially changes its dependence on k_x from the one for $k_x d \ll 1$. However,

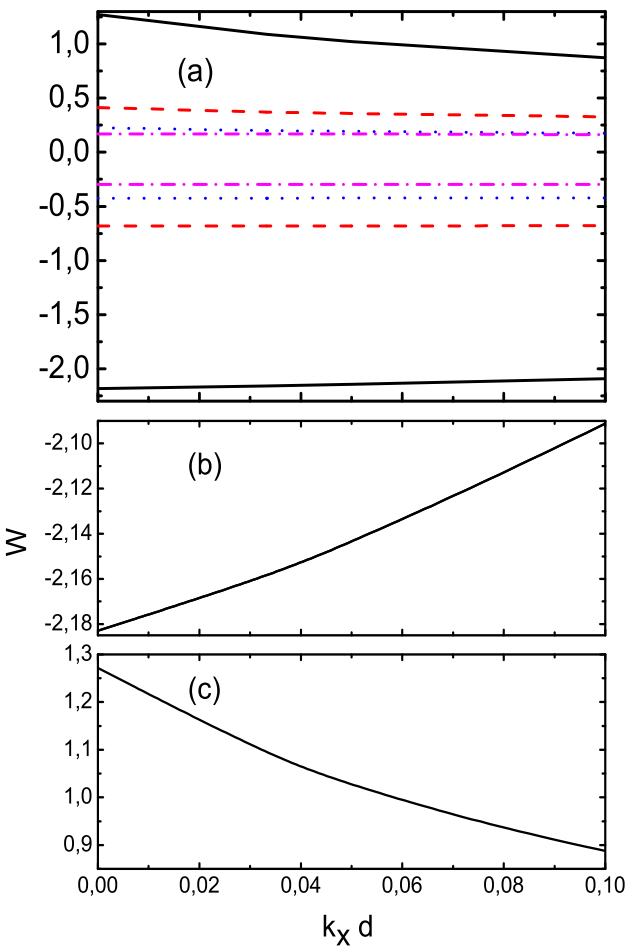

Figure 6: (Color online) Dimensionless phase velocity W as function of $k_x d$ at a long-wavelength region $0.1 \geq k_x d > 0$ for $\eta = 2$, $2M_0/B_{ext} = 0.5$, $B_{ext} = 0.6$T. Figs. 6(a), 6(b), and 6(c) show: (a) four fastest MEMPs among the modes with the positive (negative) chirality, (b) zoom for the fastest MEMP with the negative chirality, and (c) zoom for the fastest MEMP with the positive chirality.

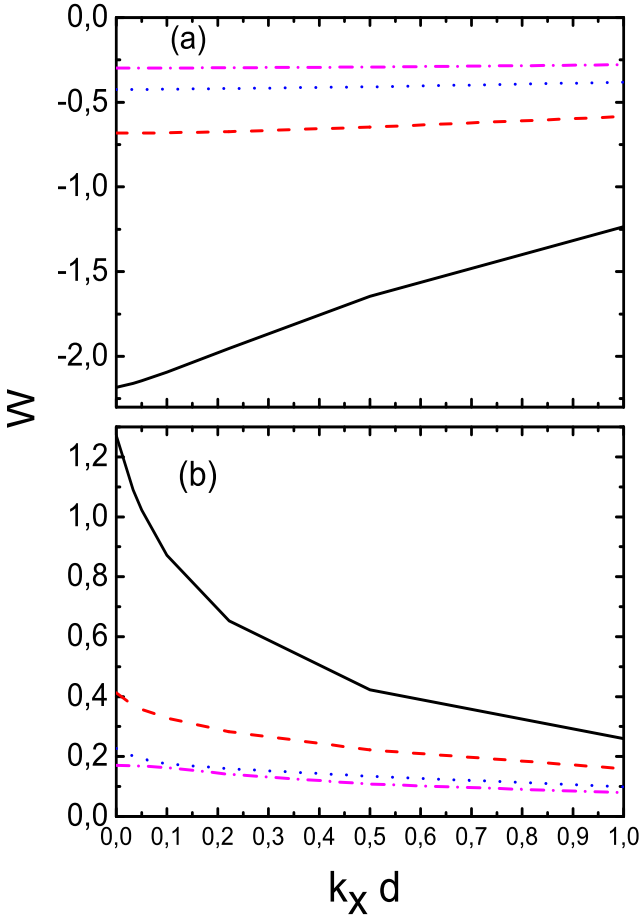

Figure 7: (Color online) Dimensionless phase velocity W as function of $k_x d$ at a wide region $1.0 \geq k_x d > 0$ for parameters of Fig. 6. Figs. 7(a) and 7(b) show four fastest MEMPs among the modes with the negative and the positive chirality, respectively.

in Fig. 7(a) the changes for $W_1^{(n)}(k_x)$ are rather small so it is still well approximated as $W_1^{(n)}(k_x) \approx 0.89\, k_x d - 2.183$ in a wide region $1.0 \geq k_x d > 0$. In addition, Fig. 7(a) shows that only at $k_x d \sim 1$ velocities $W_j^{(n)}(k_x)$, $j = 2, 3, 4$, become a weakly dependent on k_x.

In Fig. 8(a) and Fig. 8(b) we present dimensionless group velocity, $W_g(k_x)$, for MEMPs shown in Fig. 7(a) and Fig. 7(b), at the long-wavelength region $0.1 \geq k_x d > 0$. In addition, in Fig. 9(a) and Fig. 9(b) we present W_g, for MEMPs shown in Fig. 7(a) and Fig. 7(b), at a wide region $1.0 \geq k_x d > 0$.

2. *Magnetic edge magnetoplasmons for $B_{ext} < 0$, $M_0 < 0$*

In Figs. 2 - 9 we have studied MEMPs for $B_{ext} > 0$, $M_0 > 0$ which give $v_0 > 0$ and $B_0 > 0$ for all these figures. If we change the sign of B_{ext} and M_0 on negative then v_0 and B_0 also become negative. Further, it is seen that we again arrive to the same Figs. 2 - 9, however, now $W = \omega/v_0 k_x > 0$ due to $v_0 < 0$ will correspond to the negative chirality (as here $\omega/k_x < 0$) and $W < 0$ will correspond to the positive chirality (as here $\omega/k_x > 0$).

B. Effect of a hysteresis. Magnetic edge magnetoplasmons for $B_{ext} < 0$, $M_0 > 0$ and $B_{ext} > 0$, $M_0 < 0$.

Fig. 10 is plotted for the same positive M_0, $\eta = 1.0$, and $|B_{ext}|$ as Fig. 2, however, here $B_{ext} < 0$ and, respectively, $2M_0/B_{ext} = -0.5$. For $B_{ext} = -0.6$T this implies that $M_0 = B_{ext}^2/(4B_0) = 3/20$T for $B_0 = 0.6$T. Point out that v_0 and B_0 in Fig. 10 have the same positive values as in Fig. 2. In Fig. 10(a) we present the dispersion relations for dimensionless phase velocities, $W = W_j(k_x)$, of four fastest MEMP modes $|W_1^{(n)}| > |W_2^{(n)}| > ... > |W_4^{(n)}|$ with the negative chirality, $W < 0$, and of four fastest MEMP modes with the positive chiral-

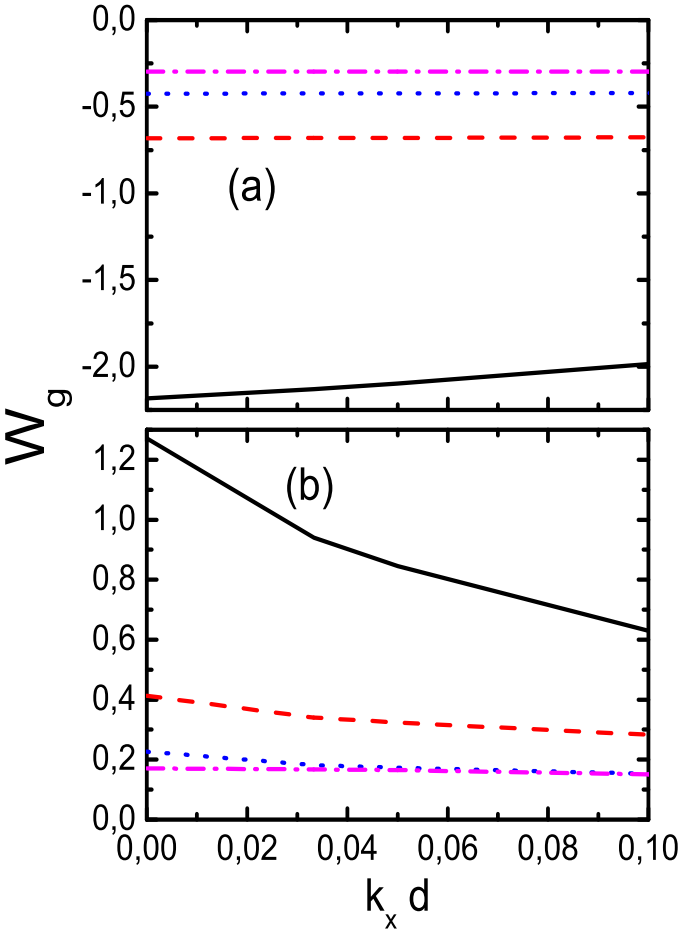

Figure 8: (Color online) Dimensionless group velocity W_g as function of $k_x d$ at a long-wavelength region $0.1 \geq k_x d > 0$ for the eight waves of Fig. 6

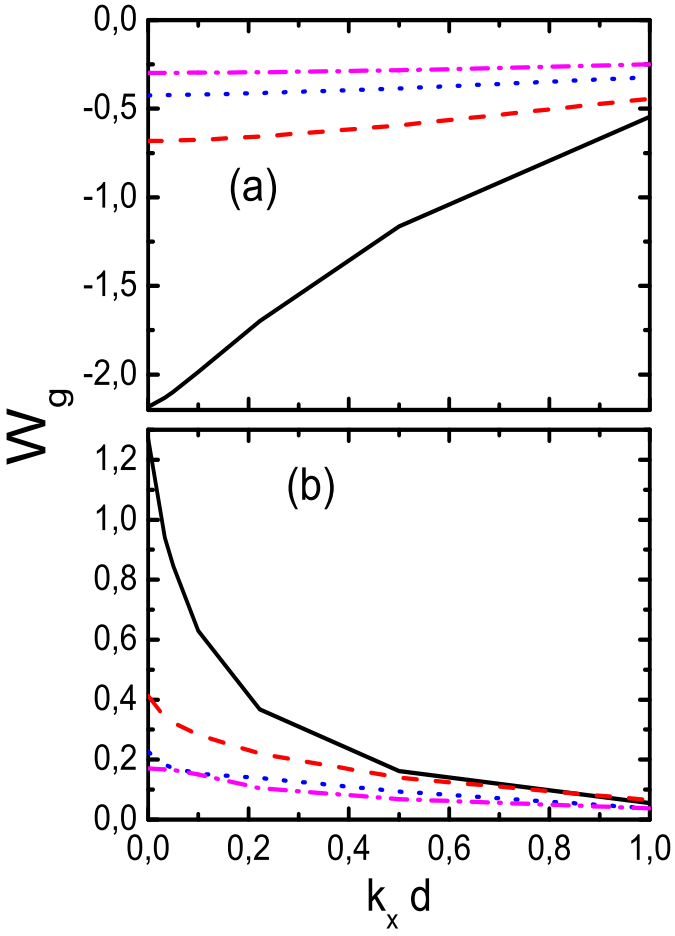

Figure 9: (Color online) Dimensionless group velocity W_g as function of $k_x d$ at $1.0 \geq k_x d > 0$ for parameters of Fig. 6. Fig. 9(a) and Fig. 9(b) show MEMPs with the negative and the positive chirality.

ity, $W_1^{(p)} > W_2^{(p)} > ... > W_4^{(p)} > 0$ at a long-wavelength region $k_x d \ll 1$. Fig. 10(b) presents a zoom of the dispersion relation $W_1^{(n)}(k_x) \approx 0.50\, k_x d - 1.373$. According to Fig. 10(a), the rest MEMPs of the negative chirality have negligible spatial dispersion in the long-wavelength region. Fig. 10(c) presents a zoom of the dispersion relation $W_1^{(p)}(k_x) \approx -1.59\, k_x d + 0.494$; it is much steeper than in Fig. 10(b). From comparison of Fig. 10(b) and Fig. 10(c) with Figs. 2(b), 2(c) it is seen that the velocity of the fastest MEMP with the negative chirality ($W < 0$) only weakly decreases, about 3%, for a reversed sign of B_{ext} as the velocity of the fastest MEMP with the positive chirality decreases much stronger, more than 30%.

In Fig. 11 dimensionless phase velocity W is plotted for a wider region of $k_x d$ than in Fig. 10; parameters are the same as in Fig. 10. In Fig. 11(b) two anti-crossings for phase velocities are clearly seen for $k_x d < 0.3$: one at $k_x d \approx 0.1$ and another at $k_x d \approx 0.2$.

In Figs. 10 - 11 we have studied MEMPs for $B_{ext} < 0$, $M_0 > 0$ which give $v_0 > 0$, $B_0 > 0$, and $2M_0/B_{ext} = -0.5$ for these figures. If we change the sign of B_{ext} on positive and and the sign of M_0 on negative then both v_0 and B_0 become negative. Let us assume that the absolute values of parameters are the same as in Figs. 10 - 11. Then it is seen that we will obtain the same Figs. 10 - 11, however, where now $W = \omega/v_0 k_x > 0$ due to $v_0 < 0$ will correspond to the negative chirality ($\omega/k_x < 0$) and $W < 0$ will correspond to the positive chirality ($\omega/k_x > 0$).

IV. CONCLUDING REMARKS

We have shown that HPMG strongly changes properties of MEMPs. In particular, they obtained spatial dispersion of unconventional form in the long-wavelength region, $k_x d \leq 0.1$. Where for two most fast MEMPs the phase velocities $\omega_1^{(n,p)}(k_x)/k_x \approx (a_{n,p} k_x + b_{n,p})$. In a wider region $1 \geq k_x d \geq 0$ the phase velocity of most fast MEMP (with the negative chirality, $W^{(n)} < 0$, $b_n < 0$) still rather closely follow the same linear behaviour, $\omega_1^{(n)}(k_x)/k_x \approx (a_n k_x + b_n)$, e.g., see Figs. 3(a), 7(a), 11(a). However, the phase velocity of second most fast

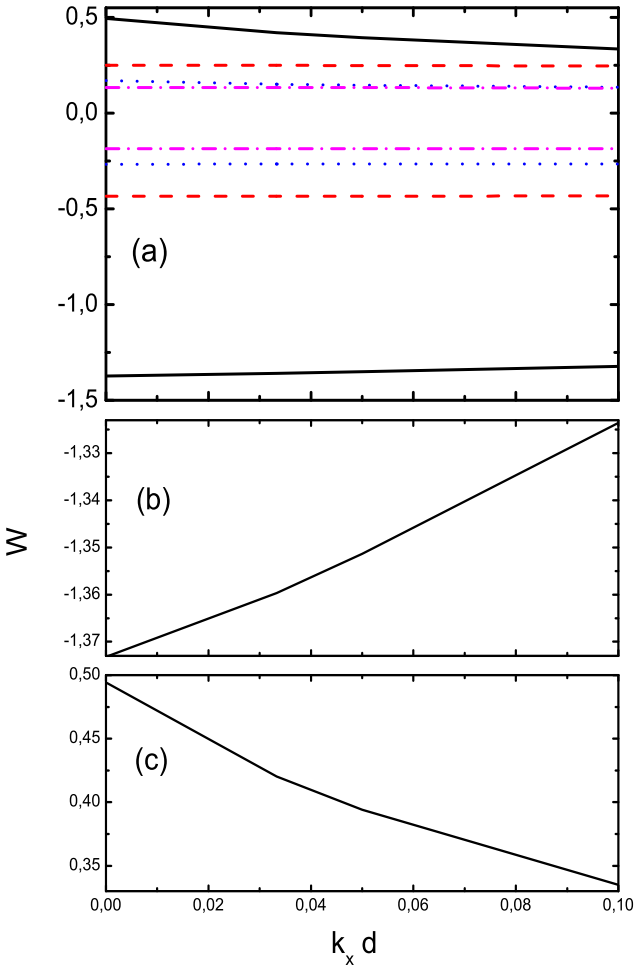

Figure 10: (Color online) Dimensionless phase velocity $W = \omega/k_x v_0$ as function of $k_x d$ at a long-wavelength region $0.1 \geq k_x d > 0$ for $\eta = 1$, $2M_0/B_{ext} = -0.5$, $B_{ext} = -0.6$T, $v_0 > 0$. Figs. 10(a), 10(b), and 10(c) show: (a) four fastest MEMPs among the modes with the positive (negative) chirality, (b) zoom for the fastest MEMP with the negative chirality, and (c) zoom for the fastest MEMP with the positive chirality.

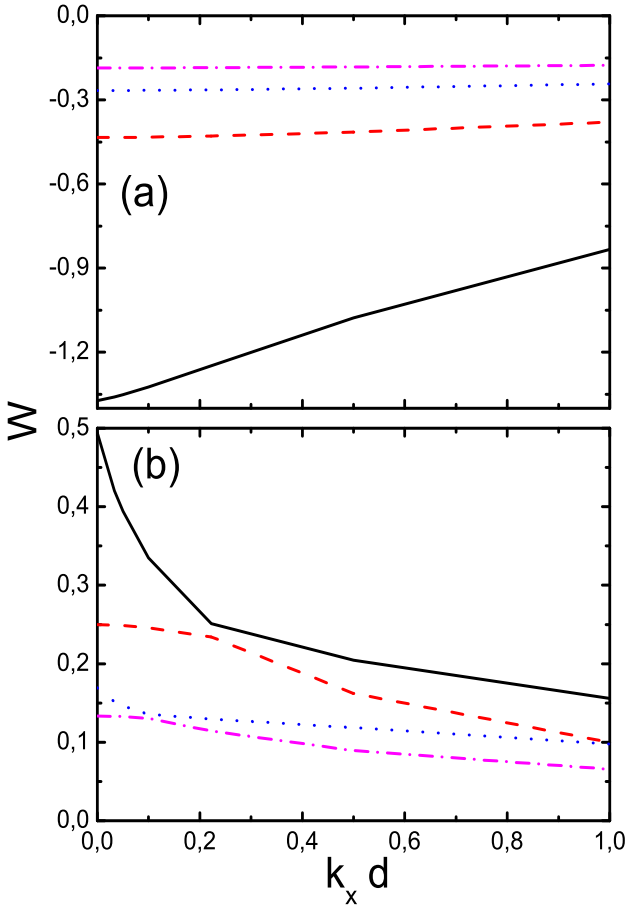

Figure 11: (Color online) Dimensionless phase velocity W as function of $k_x d$ at a wide region $1.0 \geq k_x d > 0$ for parameters of Fig. 10. Figs. 11(a) and 11(b) show four fastest MEMPs among the modes with the negative and the positive chirality, respectively. In Fig. 11(b) three anti-crossings are seen.

MEMP (with the positive chirality, $W^{(p)} > 0$, $b_p > 0$) for $1 \geq k_x d \geq 0.1$ shows behaviour of $\omega_1^{(p)}(k_x)/k_x$ essentially different from $\approx (a_p k_x + b_p)$, e.g., see Figs. 3(b), 7(b), 11(b).

Point out, two most fast MEMPs $\omega_1^{(n,p)}(k_x)$ propagate in opposite directions along the magnetic edge, with a strong overlap and localization of their spatial structures at the edge region. Then appearance of essential imperfections (e.g., they can be created on purpose) at the ends of a segment of length Λ_x along the magnetic edge will create a coupling at these ends between both MEMPs and at some resonance frequency ω_r a closed wave path within the section Λ_x. If the phase shift due to reflection at the ends of the section is negligible and the wave vectors $k_x^{(n),(p)} > 0$ are so small that $\omega_r \approx |b_n| k_x^{(n)} = b_p k_x^{(p)}$ then from $(k_x^{(n)} + k_x^{(p)})\Lambda_x = 2\pi N$, with $N = 1, 2, ...$, we obtain that

$$k_x^{(n)} = \frac{b_p}{|b_n|} k_x^{(p)} = \frac{2\pi N b_p}{\Lambda_x(|b_n| + b_p)}. \qquad (15)$$

In our model, see Fig. 1, we assume that HPMG is given by the half-plane metallic nonmagnetic film of negligible thickness, ($y < 0$, $z = d$), and that 2DES is embedded in GaAs based sample. Notice, for a real experimental setup a finite thickness of HPMG can be treated as negligible if it is much smaller than d, and ηd. Besides HPMG and the plane of 2DES the rest of space we assume as a dielectric background with spatially homogeneous (and real) dielectric constant ε; i.e., the ferromagnetic semi-infinite film is a dielectric one with dielectric constant $\varepsilon \approx 12.5$. Point out, such ferromagnetic materials as ferrite or ceramic magnets can show both dielectric and ferromagnetic properties similar to ones assumed in present study.

In addition, the properties of MEMPs for the present model, at $\eta \leq 1$ (especially for $\eta \ll 1$), should be similar to the properties of MEMPs of more easily experimentally realised setup with the ferromagnetic semi-infinite

film, as in Fig. 1, that is also *metallic* and placed on a top of GaAs sample (with the rest of a space filled in, e.g., with the dielectric medium with the same dielectric constant as GaAs, except the $z = 0$ plane of 2DES). In this case the ferromagnetic semi-infinite film can be made, e.g., from Dysprosium (Dy) or Permalloy that at liquid helium temperature $T = 4.2$K will show necessary ferromagnetic properties and, due to their metallic behaviour, well approximate the effect of HPMG. The decrease of η between 1 to 0.1 will mainly lead, e.g., to a decrease of $|W_1^{(n),(p)}(k_x = 0)| \propto \eta$; so that for $\eta = 0.1$ (other parameters are the same as in Fig. 2) it follows $W_1^{(n)}(k_x) = 0.07k_xd - 0.210$ and $W_1^{(p)}(k_x) = 0.085 - 0.20k_xd$. This decrease of η has minor effect on the spatial structure of MEMPs or a form of lateral inhomogeneity of the magnetic field at the 2DES plane; however, it essentially decreases the characteristic amplitude of the latter modulation; the latter decrease becomes $\propto \eta$. for $\eta^2 \ll 1$. Point out for 2DES with the density $n_I \approx 2\times10^{11}cm^{-2}$ in GaAs based heterostructure at $T = 4.2$K usually the mobility $u = |e|\tau/m^* \approx 10^6 cm^2/Vs$. Then the condition of the strong magnetic field $\omega_c(y)\tau \gg 1$ gives $|B(y)| \gg 0.01$T; in addition, from Eq. (1), for $\eta \leq 2$, it follows that this condition reduces to $|B_{ext}| \gg 0.01$T.

Present MEMPs are slow, $\omega/k_x \ll c/\sqrt{\varepsilon}$, potential waves; as η v_0 is a characteristic phase velocity of the MEMPs, this condition obtains the form $B_{ext}^2 \gg 4\eta|e|n_I M_0/\sqrt{\varepsilon}$. In addition, the results reported in this work, for $k_xd \leq 1$, assume that $v_0 \ll \omega_c(y)d$ and a strong magnetic moment, $2|e|M_0/m^*c \gg \omega \cdot k_xd$.

Acknowledgments

This work was supported by the Brazilian FAPEAM (Fundação de Amparo à Pesquisa do Estado do Amazonas) Grants: Universal Amazonas (Edital 021/2011), O. G. B., and PVS (Pesquisador Visitante Senior), I. A. L. Also support, I. A. L., by funding from the European Union Seventh Framework Programme (FP7/2007-2013) under grant agreement nº PCOFUND-GA-2009-246542 and the Foundation for Science and Technology of Portugal is acknowledged.

Appendix A: Matrix elements

$$I_{mn}^{(1)} = \frac{\pi}{2}\int_0^1 dX \cos(m\pi X)\int_0^1 dX' \left[\cos(n\pi X') - \frac{1}{2}\delta_{n,0}\right] \times \left[\frac{1+\eta}{1+\eta(2+\eta)\cos^2(\pi X'/2)} - 1\right]\{f_0(X')\,[\Delta_\varphi(k_x, X, X') + \Delta_\varphi(k_x, -X, X')] + f_0(-X') \times [\Delta_\varphi(k_x, X, -X') + \Delta_\varphi(k_x, -X, -X')]\}, \quad \text{(A1)}$$

where $m \leq N_0$, $n \leq N_0$;

$$I_{mn}^{(2)} = \frac{\pi}{2}\int_0^1 dX \sin[(m-N_0)\pi X]\int_0^1 dX' \left[\cos(n\pi X') - \frac{1}{2}\delta_{n,0}\right]\left[\frac{1+\eta}{1+\eta(2+\eta)\cos^2(\pi X'/2)} - 1\right]\{f_0(X') \times [\Delta_\varphi(k_x, X, X') - \Delta_\varphi(k_x, -X, X')] + f_0(-X') \times [\Delta_\varphi(k_x, X, -X') - \Delta_\varphi(k_x, -X, -X')]\}, \quad \text{(A2)}$$

where $m \geq N_0 + 1$, $n \leq N_0$;

$$I_{mn}^{(3)} = \frac{\pi}{2}\int_0^1 dX \cos(m\pi X)\int_0^1 dX' \sin[(n-N_0)\pi X'] \times \left[\frac{1+\eta}{1+\eta(2+\eta)\cos^2(\pi X'/2)} - 1\right]\{f_0(X')\,[\Delta_\varphi(k_x, X, X') + \Delta_\varphi(k_x, -X, X')] - f_0(-X') \times [\Delta_\varphi(k_x, X, -X') + \Delta_\varphi(k_x, -X, -X')]\}, \quad \text{(A3)}$$

where $m \leq N_0$, $n \geq N_0 + 1$;

$$I_{mn}^{(4)} = \frac{\pi}{2}\int_0^1 dX \sin[(m-N_0)\pi X]\int_0^1 dX' \sin[(n-N_0)\pi X'] \times \left[\frac{1+\eta}{1+\eta(2+\eta)\cos^2(\pi X'/2)} - 1\right]\{f_0(X')\,[\Delta_\varphi(k_x, X, X') - \Delta_\varphi(k_x, -X, X')] - f_0(-X') \times [\Delta_\varphi(k_x, X, -X') - \Delta_\varphi(k_x, -X, -X')]\}, \quad \text{(A4)}$$

where $m \geq N_0 + 1$, $n \geq N_0 + 1$.

[1] V. A. Volkov and S. A. Mikhailov, *Zh. Eksp. Teor. Fiz.* **94**, 217 (1988) [*Sov. Phys. JETP* **67**, 1639 (1988)]

[2] V. A. Volkov and S. A. Mikhailov, *Electrodynamics of Two-Dimensional Electron Systems in High Magnetic Fields*, in *Landau Level Spectroscopy, Modern Problems in Condensed Matter Sciences*, Ed. by G. Landwehr and E. I. Rashba (North-Holland, Amsterdam 1991) vol 27.2, chapter 15, pp 855-907.

[3] M. S. Kushwaha, *Surface Science Reports* **41**, pp 1-416 (2001).

[4] R. C. Ashoori, H. L. Stormer, L. N. Pfeiffer, K. W. Baldwin, and K. West, Phys. Rev. B **45**, 3894 (1992).

[5] I. L. Aleiner and L. I. Glazman, Phys. Rev. Lett. **72**, 2935 (1994).

[6] N. B. Zhitenev, R. J. Haug, K. von Klitzing, and K. Eberl, Phys. Rev. B **52**, 11277 (1995); G. Ernst, N. B. Zhitenev, R. J. Haug, K. von Klitzing, Physica E **1**, 95 (1997).

[7] G. Ernst, R. J. Haug, J. Kuhl, K. von Klitzing, and K. Eberl, Phys. Rev. Lett. **77**, 4245 (1996).

[8] O. G. Balev and P. Vasilopoulos, Phys. Rev. B **56**, 13252 (1997).

[9] O. G. Balev and P. Vasilopoulos, Phys. Rev. Lett. **81**, 1481 (1998); O. G. Balev, P. Vasilopoulos, and Nelson Studart, J. Phys.: Condens. Matt. **11**, 5143 (1999).

[10] O. G. Balev and P. Vasilopoulos, Phys. Rev. B **59**, 2807 (1999).

[11] G. Sukhodub, F. Hohls, and R. J. Haug, Phys. Rev. Lett. **93**, 196801 (2004).

[12] M. N. Khannanov, A. A. Fortunatov and I. V. Kukushkin, *Pis'ma Zh. Eksp. Teor. Fiz.* **90**, 740 (2009) [*JETP Lett.* **90**, 667 (2009)].

[13] S. Silva and O. G. Balev, J. Appl. Phys. **107**, 104310 (2010).

[14] I. V. Andreev, V. M. Muravev, D. V. Smetnev, and I. V. Kukushkin, Phys. Rev. B **86**, 125315 (2012).

[15] I. V. Andreev, V. M. Muravev, and I. V. Kukushkin, *Pis'ma Zh. Eksp. Teor. Fiz.* **96**, 588 (2012) [*JETP Lett.* **96**, 536 (2012)].

[16] E. Bocquillon, V. Freulon, J-. M. Berroir, P. Degiovanni, B. Placais, A. Cavanna, Y. Jin, and G. Feve, Nat. Commun. **4**, 1839 (2013).

[17] K.-i. Sasaki, S. Murakami, Y. Tokura, and H. Yamamoto, Phys. Rev. B **93**, 125402 (2016).

[18] O. G. Balev, P. Vasilopoulos, and H. O. Frota, Phys. Rev. B **84**, 245406 (2011).

[19] O. G. Balev, A. C. A. Ramos, and H. O. Frota, Phys. Rev. B **85**, 205421 (2012).

[20] O. G. Balev, and A. C. A. Ramos, AIP Advances **2**, 042161 (2012).

[21] W. Wang, J. M. Kinaret, and S. P. Apell, Phys. Rev. B **85**, 235444 (2012).

[22] W. Wang, S. P. Apell, and J. M. Kinaret, Phys. Rev. B **86**, 125450 (2012).

[23] I. Petkovic, F. I. B. Williams, K. Bennaceur, F. Portier, P. Roche, and D. C. Glattli, Phys. Rev. Lett. **110**, 016801 (2013).

[24] N. Kumada, S. Tanabe, H. Hibino, H. Kamata, M. Hashisaka, K. Muraki, and T. Fujisawa, Nat. Commun. **4**, 1363 (2013).

[25] N. Kumada, P. Roulleau, B. Roche, M. Hashisaka, H. Hibino, I. Petkovic, and D. C. Glattli, Phys. Rev. Lett. **113**, 266601 (2014).

[26] Balev O. G. and Larkin I. A., *J. Phys.; conf. Ser.* **456**, 012023 (2013).

[27] Balev O. G. and Larkin I. A., *J. Phys.; conf. Ser.* **510**, 012034 (2014).

[28] J. D. Jackson, *Classical Electrodynamics*, 3d ed. (John Wiley&Sons, New York, 1999).

[29] Lloyd W. Engel, Brenden Magill, private communication, unpublished.

[30] O. G. Balev and Nelson Studart, Phys. Rev. B **61**, 2703 (2000).

[31] L. D. Landau and E. M. Lifshitz, *Eletrodynamics of Continuous Media* (Pergamon Press, Oxford, 1960).